nature medicine

LETTERS

https://doi.org/10.1038/s41591-018-0254-9

A CD4+ T cell population expanded in lupus blood provides B cell help through interleukin-10 and succinate

Simone Caielli[1,2,3], Diogo Troggian Veiga[4], Preetha Balasubramanian[2,3], Shruti Athale[1], Bojana Domic[1], Elise Murat[1,2,3], Romain Banchereau[1], Zhaohui Xu[1], Manjari Chandra[1], Cheng-Han Chung[4], Lynnette Walters[1,5], Jeanine Baisch[1,2,3], Tracey Wright[5,6], Marilynn Punaro[5,6], Lorien Nassi[5,6], Katie Stewart[5,6], Julie Fuller[5,6], Duygu Ucar[4], Hideki Ueno[1,7], Joseph Zhou[8], Jacques Banchereau[4,9] and Virginia Pascual[1,2,3,5,9*]

Understanding the mechanisms underlying autoantibody development will accelerate therapeutic target identification in autoimmune diseases such as systemic lupus erythematosus (SLE)[1]. Follicular helper T cells (T_{FH} cells) have long been implicated in SLE pathogenesis. Yet a fraction of autoantibodies in individuals with SLE are unmutated, supporting that autoreactive B cells also differentiate outside germinal centers[2]. Here, we describe a CXCR5$^-$CXCR3$^+$ programmed death 1 (PD1)^{hi}CD4$^+$ helper T cell population distinct from T_{FH} cells and expanded in both SLE blood and the tubulointerstitial areas of individuals with proliferative lupus nephritis. These cells produce interleukin-10 (IL-10) and accumulate mitochondrial reactive oxygen species as the result of reverse electron transport fueled by succinate. Furthermore, they provide B cell help, independently of IL-21, through IL-10 and succinate. Similar cells are generated in vitro upon priming naive CD4$^+$ T cells with plasmacytoid dendritic cells activated with oxidized mitochondrial DNA, a distinct class of interferogenic toll-like receptor 9 ligand[3]. Targeting this pathway might blunt the initiation and/or perpetuation of extrafollicular humoral responses in SLE.

Activation of plasmacytoid dendritic cells (pDCs) with either chromatin-containing immune complexes[4,5] or neutrophil-derived oxidized mitochondrial DNA (mtDNA)[3] leads to type I interferon (IFN) production. As antigen-presenting cells, pDCs also shape adaptive immune responses[6,7]. Indeed, pDC activation with CpGA induces naive CD4$^+$ T cells to become regulatory (type 1 regulatory T cells)[8]. Mechanistically, CpGA activates interferon regulatory factor 7 (IRF7)-related pathways but only minimally activates nuclear factor κB (NF-κB)-related pathways[9], as detected by lower expression of interleukin-6 (IL-6) and CD86 as well as decreased p65 nuclear translocation compared with CpGB (Fig. 1a,b and Supplementary Fig. 1a–c). Oxidized mtDNA exclusively triggers IFN production. Like CpGA, it upregulates major histocompatibility antigens (human leukocyte antigens (HLAs)), CD83 and CD40 (Fig. 1a,b and Supplementary Fig. 1a–d). However, it uniquely induces the IL-3 receptor α-chain (CD123), which upon engagement with IL-3 promotes pDC survival[10] (Fig. 1b and Supplementary Fig. 1e). Activation of pDCs with either CpGA or oxidized mtDNA downregulates expression of the chemokine receptors CXCR4 and CXCR3 while increasing CCR7, which promotes migration to secondary lymphoid organs[11] (Fig. 1b and Supplementary Fig. 1f).

To explore the biological outcome of activating pDCs with these two different toll-like receptor 9 ligands, we cocultured either type of activated pDC with naive CD4$^+$ T cells (hereafter referred to as CpGA CD4$^+$ T cells and oxidized mtDNA CD4$^+$ T cells, respectively). As a control we used naive CD4$^+$ T cells activated with anti-CD3/CD28 antibodies (hereafter referred to as T_H0 cells). Upon sorting and restimulating proliferating (carboxyfluorescein diacetate succinimidyl ester (CFSE)^{lo}) CD4$^+$ T cells (Supplementary Fig. 2a), CpGA and oxidized mtDNA CD4$^+$ T cells expressed similar proinflammatory chemokine receptors and cytotoxic molecules. They also produced high levels of IFN-γ and low levels of IL-2 (Fig. 1c,d and Supplementary Fig. 2b). Oxidized mtDNA CD4$^+$ T cells, however, secreted significantly higher levels of IL-10 and IL-3 (Fig. 1c,d and Supplementary Fig. 2c).

In agreement with the reported type 1 helper T cell (T_H1 cell) origin of IFN-γ$^+$IL-10$^+$ T cells, both CpGA and oxidized mtDNA CD4$^+$ T cells expressed the T_H1-associated transcription factors T-bet (encoded by *TBX21*) and EOMES[12] as well as the chemokine receptor CXCR3[13] (Fig. 1c and Supplementary Fig. 2d). Furthermore, knockdown of *TBX21* substantially decreased the generation of IFN-γ$^+$IL-10$^+$CD4$^+$ T cells. (Supplementary Fig. 2e).

CpGA-activated pDCs induce anergic CD4$^+$ T cells[8]. Accordingly, CpGA CD4$^+$ T cells proliferated poorly upon reactivation (Fig. 1e and Supplementary Fig. 2f). Lack of expression of D-type cyclins and failure to phosphorylate the retinoblastoma tumor suppressor protein (p-Rb) suggested their arrest in the cell cycle G1 phase[14] (Supplementary Fig. 2g). On the contrary, oxidized mtDNA CD4$^+$ T cells proliferated vigorously upon reactivation and expressed D-type cyclins and p-Rb (Fig. 1e and Supplementary Fig. 2f,g).

[1]Baylor Institute for Immunology Research, Dallas, TX, USA. [2]Drukier Institute for Children's Health, Weill Cornell Medicine, New York, NY, USA. [3]Department of Pediatrics, Weill Cornell Medicine, New York, NY, USA. [4]The Jackson Laboratory for Genomic Medicine, Farmington, CT, USA. [5]Texas Scottish Rite Hospital for Children, Dallas, TX, USA. [6]Department of Pediatrics, University of Texas Southwestern Medical Center, Dallas, TX, USA. [7]Mount Sinai School of Medicine, New York, NY, USA. [8]Pathologists Bio-Medical Laboratories, Lewisville, TX, USA. [9]These authors contributed equally to this work: Jacques Banchereau, Virginia Pascual. *e-mail: vip2021@med.cornell.edu

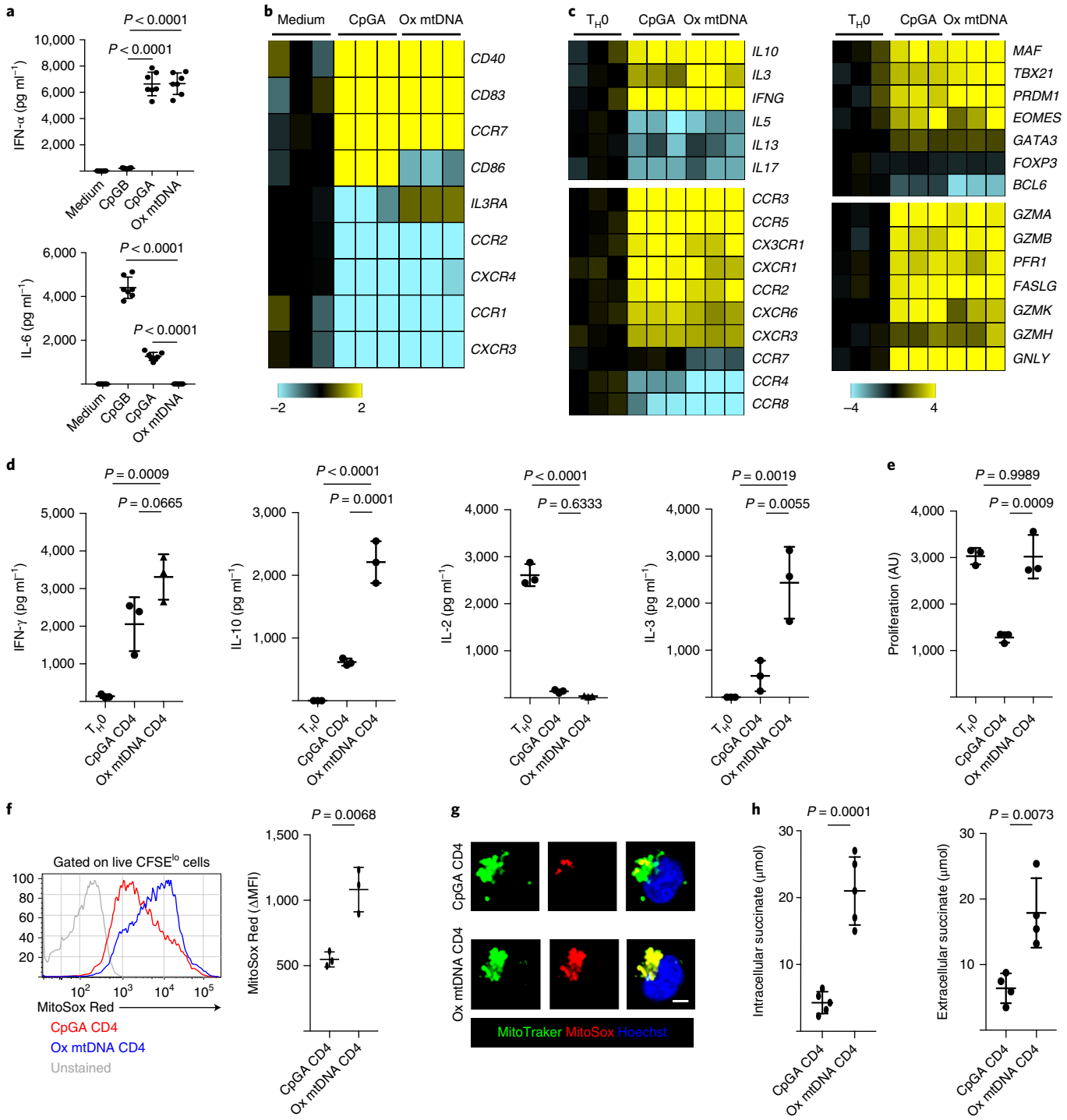

Fig. 1 | Oxidized mtDNA induces a unique pDC phenotype. a, Cytokine profile of pDCs activated for 24 h with medium, CpGB, CpGA or oxidized mtDNA ($n = 7$ independent experiments). **b**, Gene expression profile of pDCs in response to CpGA or oxidized mtDNA ($n = 3$ independent experiments). **c**, Gene expression profile of T_H0, CpA and oxidized mtDNA CD4$^+$ T cells ($n = 3$ independent experiments). For the gene expression profiles, the colored key shows fold change in gene expression. **d**,**e**, Cytokine profile (**d**) and proliferation (**e**) of T_H0, CpGA or oxidized mtDNA CD4$^+$ T cells upon reactivation with CD3/CD28 ($n = 3$ independent experiments). **f**,**g**, mtROS production by CpGA or oxidized mtDNA CD4$^+$ T cells was assessed by flow cytometry (**f**; $n = 3$ independent experiments) or by immunofluorescence microscopy (**g**; 1 representative of 3 independent experiments). MFI, mean fluoresence intensity. Scale bar, 7 μm. **h**, Intracellular (left) and extracellular (right) succinate levels in CpGA or oxidized mtDNA CD4$^+$ T cells ($n = 5$ independent experiments). Shown are mean ± s.e.m.; statistical analysis by nonparametric one-way ANOVA (**a**–**e**) and two-tailed nonparametric unpaired *t*-test at 95% confidence interval (CI) (**f**,**h**). Ox, oxidized.

As reported for proliferating CD4$^+$ T cells[15], oxidized mtDNA CD4$^+$ T cells produced higher mitochondrial reactive oxygen species (mtROS) levels than CpGA CD4$^+$ T cells (Fig. 1f,g and Supplementary Fig. 3a), and treatment with MitoTempo attenuated their proliferation (Supplementary Fig. 3b,c). Complex I of the electron-transport chain is the major site for mtROS production during

reverse electron transport (RET), an event characterized by mtROS-mediated disintegration of complex I[16]. Indeed, complex I levels were reduced in an mtROS- and mitochondrial protease-dependent manner in oxidized mtDNA CD4+ T cells (Supplementary Fig. 3d–f). Complex I degradation leads to decreased complex I–mediated respiration[17] (Supplementary Fig. 3g), which can be compensated by higher complex II activity (Supplementary Fig. 3h). Indeed, we detected similar maximal respiration rates in CpGA and oxidized mtDNA CD4+ T cells (Supplementary Fig. 3i). RET is induced upon succinate accumulation[18]. Accordingly, oxidized mtDNA CD4+ T cells produced and secreted higher levels of succinate than CpGA CD4+ T cells (Fig. 1h). As succinate accumulation leads to hypoxia-inducible factor 1α (HIF-1α) stabilization[19], HIF-1α was upregulated in oxidized mtDNA compared with CpGA CD4+ T cells (Supplementary Fig. 4a).

Constitutive activation of mechanistic target of rapamycin (mTOR) in systemic lupus erythematosus (SLE) T cells leads to ROS production[20]. As expected, rapamycin reduced the ability of naive CD4+ T cells to proliferate and differentiate into IFN-γ+IL-10+ T cells in response to oxidized mtDNA-activated pDCs (Supplementary Fig. 4b). Decreased proliferation as well as mtROS and cytokine production also occurred upon restimulation of oxidized mtDNA CD4+ T cells in the presence of rapamycin (Supplementary Fig. 4c).

In line with their capacity to produce high IL-10 levels, oxidized mtDNA CD4+ T cells support IL-10-dependent differentiation of naive B cells into plasmablasts[21,22] (Fig. 2a,b). Contrary to T_{FH} cells[23], however, these cells do not express CXCR5, Bcl-6 or IL-21 (Supplementary Fig. 5a,b). Instead, CXCR4 expression suggests a role in extrafollicular B cell responses. Yet, CpGA CD4+ T cells also produce IL-10 but are weaker B cell helpers. Because succinate modulates immune functions upon binding to the succinate receptor (SUCNR1)[24], which is expressed by all major human blood B cell subsets (Fig. 2c), we tested its B cell helper capacity. Indeed, blocking SUCNR1 partially inhibited oxidized mtDNA CD4+ T cell–driven B cell activation (Fig. 2d). Importantly, high levels of immunoglobulin M (IgM) and IgG were detected in cocultures of CpGA CD4+ T cells and B cells supplemented with succinate (Supplementary Fig. 5c). Finally, succinate synergized with IL-10 in promoting immunoglobulin secretion by naive B cells activated in vitro with CD40L (Supplementary Fig. 5d).

To identify the signals leading to succinate accumulation in oxidized mtDNA CD4+ T cells, we analyzed expression of co-stimulatory (CD28 and inducible T cell co-stimulator) and co-inhibitory (cytotoxic T lymphocyte-associated antigen 4 and programmed death 1 (PD1)) receptors known to modulate T cell metabolism[25,26]. Oxidized mtDNA CD4+ T cells expressed higher PD1 levels (Supplementary Fig. 5e), and PD1 ligation was necessary for succinate and mtROS production as well as for acquisition of B cell helper function (Fig. 2e and Supplementary Fig. 5f–h).

As oxidized mtDNA is released upon activation of SLE neutrophils[3], we next explored whether cells with the phenotype of oxidized mtDNA CD4+ T cells were present in SLE blood. Indeed, CXCR3+PD1^{hi}CD4+ T cells were significantly expanded in the SLE memory (CD45RA−) non-T_{FH} (CXCR5−) CD4+ T cell compartment (Fig. 3a). To test their capacity to help B cells, we sorted and cocultured these cells with naive B cells. CXCR3+PD1^{lo}CD4+ T cells, CXCR3−PD1^{hi}CD4+ T cells and CD45RA−CXCR5+CD4+ T cells (T_{FH}) were used as controls (Supplementary Fig. 6a). Among them, CXCR3+PD1^{hi}CD4+ T cells and T_{FH} cells were equally effective at inducing naive and memory B cell differentiation into IgG-producing plasmablasts (Fig. 3b,c and Supplementary Fig. 6b,c).

Upon T cell receptor stimulation, SLE blood T_{FH} cells produced significant amounts of IL-21, CXCL13 and IL-2, while CXCR3+PD1^{hi}CD4+ T cells released the highest levels of IL-10 but no IL-21 or CXCL13 (Fig. 3d and Supplementary Fig. 6d). Similar results were obtained upon contact with naive or memory B cells (Supplementary Fig. 6e). Furthermore, CXCR3+PD1^{hi}CD4+ T cells produced the highest levels of IFN-γ, IL-3, mtROS and succinate (Fig. 3d–f). Neutralization of IL-10 during coculture of naive B cells with SLE blood CXCR3+PD1^{hi}CD4+ T cells or T_{FH} cells inhibited IgG secretion, while T_{FH} cell function was mainly dependent on IL-21 (refs [27,28]). Conversely, succinate receptor blockade, but not IL-21 neutralization, decreased IgG secretion in cocultures of naive B cells and CXCR3+PD1^{hi}CD4+ T cells (Fig. 3g).

We next compared the transcriptome of SLE blood CXCR3+PD1^{hi}CD4+ T cells and T_{FH} cells. Principal component analysis (PCA) revealed 1,230 differentially expressed transcripts (log[fold change] > 1.2; false discovery rate < 0.01; Fig. 3h). Among them, CXCR3+PD1^{hi}CD4+ T cells upregulated chemokine receptors such as CCR2, CCR5 and CX3CR1 (Fig. 3i and Supplementary Fig. 6f). In addition, transcripts (*GZMA*, *GZMB*, *PRF1*, *GZMH*, *GNLY*, *CTSW*, *FCRL6*, *S1PR5*, *SLAMF7* and *NKG7*) as well as transcription factors linked to cytotoxic programs[29] (*ZNF683*, *RUNX3*, *EOMES* and *TBX21*) were exclusively upregulated in CXCR3+PD1^{hi}CD4+ T cells (Fig. 3i and Supplementary Fig. 6g). Gene ontology analysis identified additional gene sets involved in cell cycle regulation, including cyclins (*CCNE2*, *CCNB1*, *CCNB2* and *CCNA2*), cyclin-dependent kinases (*CDK1*) and elongation factors (*E2F1* and *E2F2*) as the top differentially expressed genes (Supplementary Fig. 6h). Accordingly, p-Rb levels were increased in CXCR3+PD1^{hi}CD4+ T cells compared with T_{FH} cells (Supplementary Fig. 6i).

The global chromatin landscape[30] of both cell types was also markedly different, with 935 differentially accessible chromatin sites (peaks). Indeed, most sites had increased accessibility in CXCR3+PD1^{hi}CD4+ T cells. Overall, opening peaks were detected for 690 genes, with 107 upregulated in the CXCR3+PD1^{hi}CD4+ T cell transcriptome (Fig. 3j), including cytokines (*IL3*, *IL10* and *IFNG*), transcription factors (*TBX21* and *RUNX3*), proinflammatory chemokine receptors (*CCR3*, *CCR5* and *CX3CR1*) and cytolytic molecules (*GZMB*) (Supplementary Fig. 6j).

Strikingly, the frequencies of SLE blood CXCR3+PD1^{hi}CD4+ T cells and T_{FH} cells were inversely correlated (Supplementary Fig. 7a). On the contrary, CXCR3+PD1^{hi}CD4+ T cell frequency was positively correlated with IgG and IgA levels (Fig. 4a). As previously reported[31,32], plasmablasts were expanded in our subjects' blood. A correlative trend between plasmablast and CXCR3+PD1^{hi}CD4+ T cell frequencies was found, but it did not reach statistical significance (Supplementary Fig. 7b,c), most likely owing to plasmablast fragility during cryopreservation. In addition to plasmablasts, age-associated B cells (ABCs) have been reported in SLE[33,34]. This cell population was expanded in our pediatric subjects, and the frequency of these cells was correlated with that of CXCR3+PD1^{hi}CD4+ T cells (Fig. 4b,c).

Lupus nephritis (LN), which comprises several histological classes, is one of the major drivers of morbidity and mortality in SLE. As conventional markers of kidney function are not LN class specific, we asked whether blood CXCR3+PD1^{hi}CD4+ T cells would represent a LN biomarker. When correlated with clinical and laboratory data, the highest frequency and absolute numbers of blood CXCR3+PD1^{hi}CD4+ T cells were detected in individuals with no LN or with LN class not associated with lymphocytic infiltration in the kidney (LN class II; Fig. 4d and Supplementary Fig. 7d). Conversely, the lowest frequency was found in individuals with proliferative lupus nephritis (PLN; LN classes III and IV), the most severe form of LN in children. This distribution was not driven by immunosuppressive therapy (Supplementary Fig. 7e).

Because lower numbers of blood CXCR3+PD1^{hi}CD4+ T cells in PLN might reflect their migration into the kidney, tissue sections from individuals with SLE without LN and with different LN classes were analyzed by immunofluorescence. Different degrees of CD3+ T cell infiltrates were detected in the peritubular areas of a significant fraction (13/17) of PLN sections (Supplementary Fig. 7f,g). Across

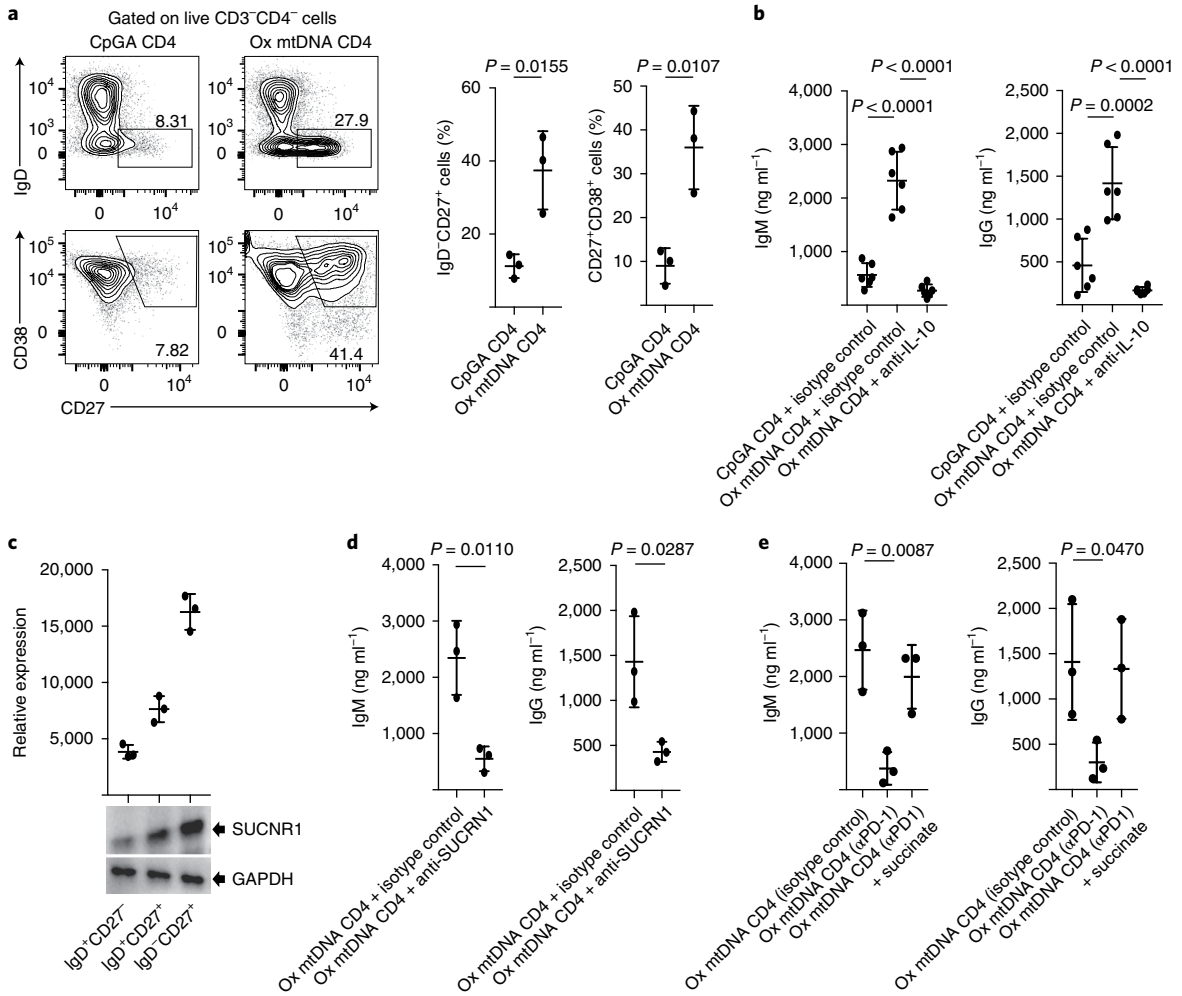

Fig. 2 | Oxidized mtDNA CD4⁺ T cells help B cells through IL-10 and succinate. a, Percentage of IgD⁻CD27⁺ and CD27⁺CD38⁺ B cells upon coculture with CpGA or oxidized mtDNA CD4⁺ T cells ($n = 3$ independent experiments). Representative flow cytometry density plots are also shown. **b**, IgM and IgG levels in the supernatants from CpGA or oxidized mtDNA CD4⁺ T cells and naive B cell cocultures ($n = 6$ independent experiments). **c**, Immunoblot analysis of SUCNR1 expression by purified human B cell subsets ($n = 3$ independent experiments). **d**, IgM and IgG levels in the supernatants from oxidized mtDNA CD4⁺ T cell and naive B cell cocultures in the presence of anti-SUCRN1 ($n = 3$ independent experiments). **e**, IgM and IgG levels in the supernatants from cocultures of oxidized mtDNA CD4⁺ T cells, generated in the presence of isotype control or anti-PD1, and naive B cells ($n = 3$ independent experiments). Shown are mean ± s.e.m.; statistical analysis by nonparametric one-way ANOVA (**b**) and two-tailed nonparametric unpaired *t*-test at 95% CI (**a**,**d**,**e**).

these PLN sections, 27.1% ± 10.3% (mean ± s.e.m.) of CD3⁺ T cells co-expressed IFN-γ and IL-10 (Fig. 4e). Although the presence of cytotoxic CD8⁺ T cells in LN has been reported[35], all infiltrating IL-10⁺ CD3⁺ T cells co-expressed CD4 (Supplementary Fig. 7h). Furthermore, similar to circulating CXCR3⁺PD1^{hi}CD4⁺ T cells, infiltrating IL-10⁺CD3⁺ T cells co-expressed PD1 (Supplementary Fig. 7i) and were positive for nitrotyrosine (mean ± s.d., 93% ± 6.1%; Fig. 4f). Because intrarenal B cells are also a feature of PLN[36], we examined the spatial relationship between IL-10⁺CD3⁺ T cells and CD20⁺ B cells. As shown in Fig. 4g, a large fraction (mean ± s.d., 43.2% ± 16%) of IL-10⁺CD3⁺ T cells appeared in close proximity to CD20⁺ B cells.

Recently, a population of CXCR5⁻PD1^{hi}CD4⁺ T cells (peripheral helper T cells (T_{PH})) was reported expanded in rheumatoid arthritis. Similar to T_{FH} cells, T_{PH} cells induce B cell differentiation and antibody secretion in an IL-21- and CXCL13-dependent manner[37]. The cells that we describe herein produce neither IL-21 nor CXCL13 and exhibit a distinctive transcriptome and chromatin landscape compared with T_{FH} cells. Importantly, they help B cells through a unique mechanism involving IL-10 and succinate.

New roles for succinate, an intermediate of the tricarboxylic acid cycle, outside metabolism have recently emerged, including its synergism with lipopolysaccharide to induce IL-1β production by macrophages[24]. The effects of succinate on innate immunity are well recognized, and this report implicates it in the shaping of adaptive immune responses as well.

B and T cells are a prominent feature of PLN infiltrates[36]. Individuals with PLN, however, carry the lowest numbers of blood CXCR3⁺PD1^{hi}CD4⁺ T cells. Instead, IFN-γ⁺IL-10⁺ROS⁺PD1^{hi}CD4⁺ T cells are found in the peritubular areas in close proximity to B cells. Of note, SUCNR1 is expressed in a variety of tissues, especially in the kidney. Within this organ, the highest receptor density is found in the proximal tubular epithelium. There, triggering of the receptor leads to release of renin from the juxtaglomerular apparatus. Consequently, succinate has been implicated in the pathogenesis of diabetic nephropathy and renovascular hypertension[38]. Whether T cell–derived succinate directly contributes to kidney damage in PLN, the main class of LN associated with renovascular hypertension, deserves further study.

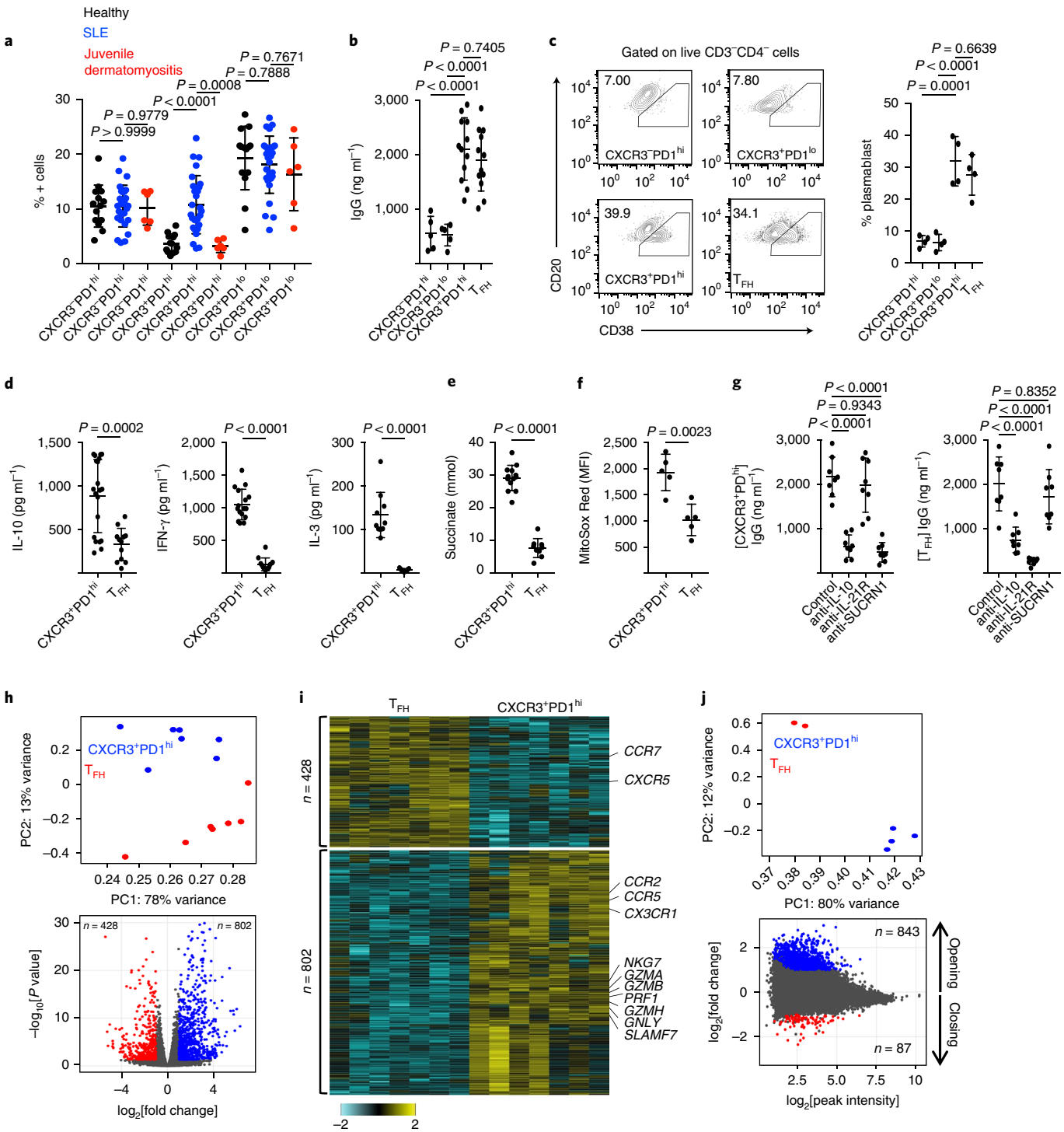

Fig. 3 | Memory CXCR5⁻CXCR3⁺PD1^{hi}CD4⁺ T cells represent the blood counterpart of oxidized mtDNA CD4⁺ T cells. a, Percentage of CXCR3⁻PD1^{hi}, CXCR3⁺PD1^{hi} and CXCR3⁺PD1^{lo}CD4⁺ T cells in the blood CD45RA⁻CXCR5⁻ compartment of healthy controls ($n=13$) and individuals with SLE ($n=27$) or juvenile dermatomyositis ($n=6$). **b**,**c**, IgG levels (**b**; $n=12$ independent experiments) and CD20/CD38 expression (**c**; $n=4$ independent experiments) on naive B cells cocultured with CXCR3⁻PD1^{hi}CD4⁺ T cells, CXCR3⁺ PD1^{hi}CD4⁺ T cells, CXCR3⁺PD1^{lo}CD4⁺ T cells or T_{FH} cells. **d**, Cytokine profile of sorted CXCR3⁺PD1^{hi}CD4⁺ T cells and T_{FH} cells ($n=18$ independent experiments). **e**,**f**, Succinate (**e**; $n=12$ independent experiments) and mtROS (**f**; $n=5$ independent experiments) levels in CXCR3⁺PD1^{hi}CD4⁺ T cells and T_{FH} cells. **g**, IgG levels in the supernatants from cocultures of CXCR3⁺PD1^{hi}CD4⁺ T cells or T_{FH} cells and naive B cells ($n=8$ independent experiments). **h**, PCA of RNA sequencing data corresponding to genes differentially expressed between CXCR3⁺PD1^{hi}CD4⁺ T cells and T_{FH} cells (top; $n=7$ independent experiments) and volcano plot of upregulated genes in each population (bottom; DESeq2, Wald test, adjusted P value < 0.05 and fold change > 2). **i**, Heat map of differentially expressed transcripts in CXCR3⁺PD1^{hi}CD4⁺ T cells and T_{FH} cells ($n=7$ independent experiments). The color scale represents the fold change in gene expression. **j**, PCA of ATAC-seq data on peaks differentially accessible between CXCR3⁺ PD1^{hi} CD4⁺ T cells (top; $n=4$ independent experiments) and T_{FH} cells ($n=2$ independent experiments). Chromatin sites with differential accessibility (bottom). Plot indicates the number of opening/closing chromatin peaks in CXCR3⁺PD1^{hi}CD4⁺ T cells compared with T_{FH} cells (EdgeR, adjusted P value < 0.05 and fold change > 2). Shown are mean ± s.e.m.; statistical analysis by nonparametric one-way ANOVA (**a–c,g**) and two-tailed nonparametric unpaired t-test at 95% CI (**d–f**). PC, principal component.

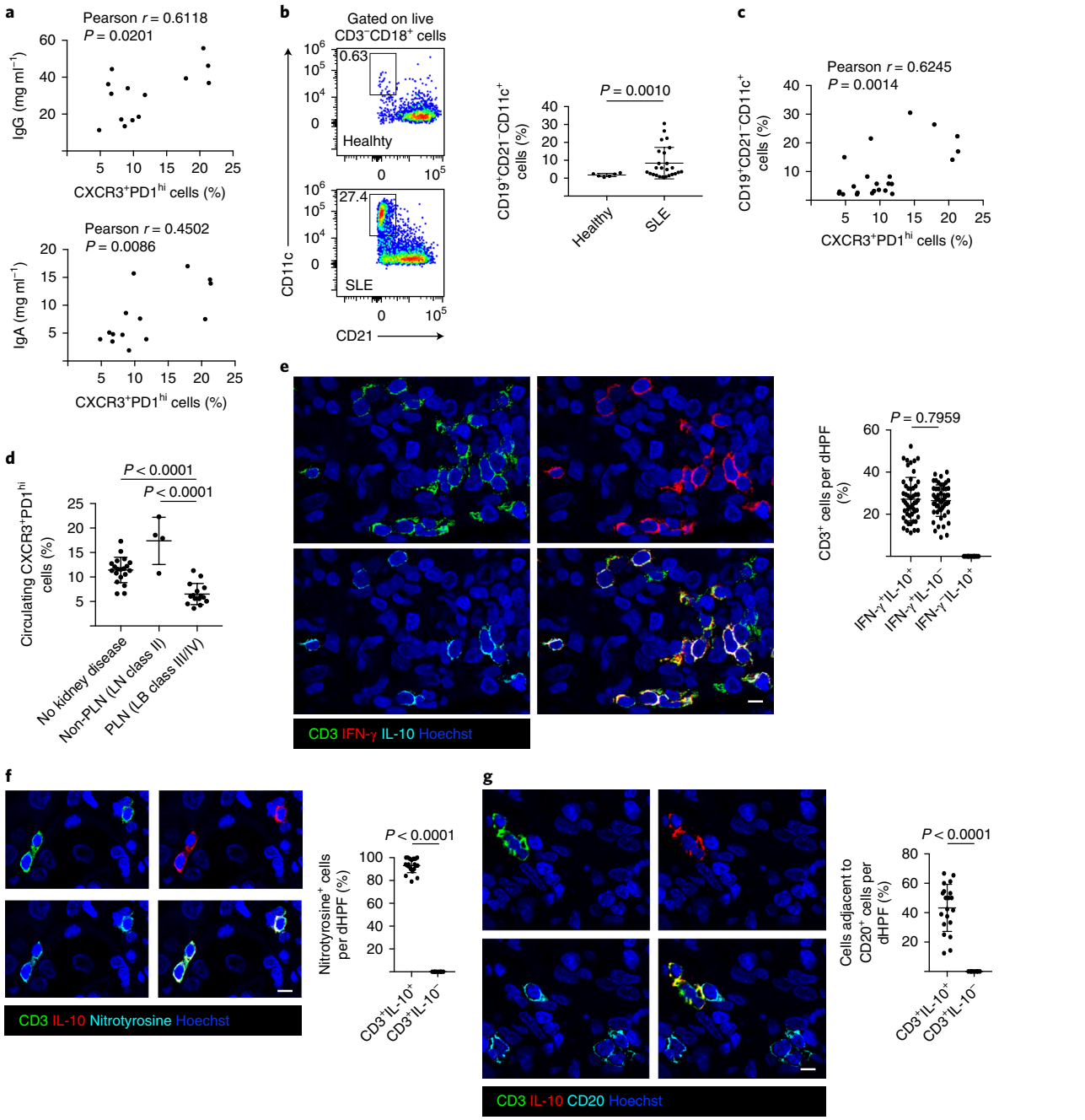

Fig. 4 | IL-10$^+$IFN-γ$^+$ROS$^+$PD1$^+$CD4$^+$ T cells accumulate in PLN lesions. a, Pearson correlation analysis between the frequency of SLE blood CXCR3$^+$PD1^{hi}CD4$^+$ T cells and serum IgG and IgA levels ($n=14$ biologically independent samples). **b**, Representative flow cytometry density plot (left) and percentage of CD19$^+$CD21$^-$CD11c$^+$ B cells (ABCs) among CD3$^-$CD19$^+$ cells (right) in the blood of healthy donors ($n=6$) or individuals with SLE ($n=25$). **c**, Pearson correlation analysis between the frequency of blood CXCR3$^+$PD1^{hi}CD4$^+$ T cells and ABCs. **d**, Percentage of CXCR3$^+$PD1^{hi}CD4$^+$ T cells in blood of individuals with SLE and class II LN ($n=4$ biologically independent samples), class III/IV LN (PLN; $n=15$ biologically independent samples) or no kidney disease ($n=20$ biologically independent samples). **e**, Representative immunofluorescence microscopy of CD3, IFN-γ and IL-10 staining in the kidney of a class IV LN section. The percentage of CD3$^+$IFN-γ$^-$IL-10$^+$, CD3$^+$IFN-γ$^+$IL-10$^-$ and CD3$^+$IFN-γ$^-$IL-10$^+$ cells is also shown ($n=10$ class III/IV LN samples; 5 digital high power field (dHPF) per sample). **f**, Representative immunofluorescence microscopy of CD3, nitrotyrosine and IL-10 staining in the kidney of a class IV LN section. The percentage of CD3$^+$IL-10$^+$nitrotyrosine$^+$ and CD3$^+$IL-10$^-$ nitrotyrosine$^+$ cells is also shown ($n=5$ class III/IV LN samples; 4 dHPF per sample). **g**, Representative immunofluorescence microscopy of CD3, IL-10 and CD20 staining in the kidney of a class IV LN section. The percentage of CD3$^+$IL-10$^+$ and CD3$^+$IL-10$^-$ cells adjacent to CD20$^+$ B cells is also shown ($n=5$ class III/IV LN samples; 4 dHPF per sample). Scale bars, 10 μm. Shown are mean ± s.e.m.; statistical analysis by nonparametric one-way ANOVA (**d**) and two-tailed nonparametric unpaired *t*-test at 95% CI (Welch's correction; **b**,**f**,**g**).

The novel CD4$^+$ T cell population that we describe, which we propose to designate as T_H10 cells, expands the spectrum of B cell helper T cells and might contribute to SLE pathogenesis and end organ damage in a variety of ways. These cells provide unique mechanistic clues for therapeutic intervention in a disease for which only one new drug has been approved in more than 60 years.

Online content

Any methods, additional references, Nature Research reporting summaries, source data, statements of data availability and associated accession codes are available at https://doi.org/10.1038/s41591-018-0254-9.

Received: 1 April 2018; Accepted: 15 October 2018;
Published online: 26 November 2018

References

1. Tsokos, G. C. Systemic lupus erythematosus. *N. Engl. J. Med.* **365**, 2110–2121 (2011).
2. Tipton, C. M. et al. Diversity, cellular origin and autoreactivity of antibody-secreting cell population expansions in acute systemic lupus erythematosus. *Nat. Immunol.* **16**, 755–765 (2015).
3. Caielli, S. et al. Oxidized mitochondrial nucleoids released by neutrophils drive type I interferon production in human lupus. *J. Exp. Med.* **213**, 697–713 (2016).
4. Guiducci, C. et al. TLR recognition of self nucleic acids hampers glucocorticoid activity in lupus. *Nature* **465**, 937–941 (2010).
5. Means, T. K. et al. Human lupus autoantibody-DNA complexes activate DCs through cooperation of CD32 and TLR9. *J. Clin. Investig.* **115**, 407–417 (2005).
6. Gilliet, M. & Liu, Y. J. Human plasmacytoid-derived dendritic cells and the induction of T-regulatory cells. *Hum. Immunol.* **63**, 1149–1155 (2002).
7. Jego, G. et al. Plasmacytoid dendritic cells induce plasma cell differentiation through type I interferon and interleukin 6. *Immunity* **19**, 225–234 (2003).
8. Ito, T. et al. Plasmacytoid dendritic cells prime IL-10-producing T regulatory cells by inducible costimulator ligand. *J. Exp. Med.* **204**, 105–115 (2007).
9. Gilliet, M., Cao, W. & Liu, Y. J. Plasmacytoid dendritic cells: sensing nucleic acids in viral infection and autoimmune diseases. *Nat. Rev. Immunol.* **8**, 594–606 (2008).
10. Grouard, G. et al. The enigmatic plasmacytoid T cells develop into dendritic cells with interleukin (IL)-3 and CD40-ligand. *J. Exp. Med.* **185**, 1101–1111 (1997).
11. Penna, G., Sozzani, S. & Adorini, L. Cutting edge: selective usage of chemokine receptors by plasmacytoid dendritic cells. *J. Immunol.* **167**, 1862–1866 (2001).
12. Glimcher, L. H. & Murphy, K. M. Lineage commitment in the immune system: the T helper lymphocyte grows up. *Genes Dev.* **14**, 1693–1711 (2000).
13. Acosta-Rodriguez, E. V. et al. Surface phenotype and antigenic specificity of human interleukin 17-producing T helper memory cells. *Nat. Immunol.* **8**, 639–646 (2007).
14. Jackson, S. K., DeLoose, A. & Gilbert, K. M. The ability of antigen, but not interleukin-2, to promote *n*-butyrate-induced T helper 1 cell anergy is associated with increased expression and altered association patterns of cyclin-dependent kinase inhibitors. *Immunology* **106**, 486–495 (2002).
15. Sena, L. A. et al. Mitochondria are required for antigen-specific T cell activation through reactive oxygen species signaling. *Immunity* **38**, 225–236 (2013).
16. Nag, S., Picard, P. & Stewart, D. J. Expression of nitric oxide synthases and nitrotyrosine during blood-brain barrier breakdown and repair after cold injury. *Lab. Investig.* **81**, 41–49 (2001).
17. Guaras, A. et al. The $CoQH_2$/CoQ ratio serves as a sensor of respiratory chain efficiency. *Cell Rep.* **15**, 197–209 (2016).
18. Murphy, M. P. How mitochondria produce reactive oxygen species. *Biochem. J.* **417**, 1–13 (2009).
19. Tannahill, G. M. et al. Succinate is an inflammatory signal that induces IL-1β through HIF-1α. *Nature* **496**, 238–242 (2013).
20. Oaks, Z., Winans, T., Huang, N., Banki, K. & Perl, A. Activation of the mechanistic target of rapamycin in SLE: explosion of evidence in the last five years. *Curr. Rheumatol. Rep.* **18**, 73 (2016).
21. Rousset, F. et al. Interleukin 10 is a potent growth and differentiation factor for activated human B lymphocytes. *Proc. Natl Acad. Sci. USA* **89**, 1890–1893 (1992).
22. Moore, K. W., de Waal Malefyt, R., Coffman, R. L. & O'Garra, A. Interleukin-10 and the interleukin-10 receptor. *Annu. Rev. Immunol.* **19**, 683–765 (2001).
23. Ueno, H., Banchereau, J. & Vinuesa, C. G. Pathophysiology of T follicular helper cells in humans and mice. *Nat. Immunol.* **16**, 142–152 (2015).
24. Mills, E. & O'Neill, L. A. Succinate: a metabolic signal in inflammation. *Trends Cell Biol.* **24**, 313–320 (2014).
25. Buck, M. D., O'Sullivan, D. & Pearce, E. L. T cell metabolism drives immunity. *J. Exp. Med.* **212**, 1345–1360 (2015).
26. Keir, M. E., Butte, M. J., Freeman, G. J. & Sharpe, A. H. PD-1 and its ligands in tolerance and immunity. *Annu. Rev. Immunol.* **26**, 677–704 (2008).
27. Locci, M. et al. Human circulating PD-1^+CXCR3^-CXCR5^+ memory T_{FH} cells are highly functional and correlate with broadly neutralizing HIV antibody responses. *Immunity* **39**, 758–769 (2013).
28. Morita, R. et al. Human blood CXCR5^+CD4^+ T cells are counterparts of T follicular cells and contain specific subsets that differentially support antibody secretion. *Immunity* **34**, 108–121 (2011).
29. Patil, V. S. et al. Precursors of human CD4^+ cytotoxic T lymphocytes identified by single-cell transcriptome analysis. *Sci. Immunol,* **3**, eaan8664 (2018).
30. Buenrostro, J. D., Giresi, P. G., Zaba, L. C., Chang, H. Y. & Greenleaf, W. J. Transposition of native chromatin for fast and sensitive epigenomic profiling of open chromatin, DNA-binding proteins and nucleosome position. *Nat. Methods* **10**, 1213–1218 (2013).
31. Arce, E. et al. Increased frequency of pre-germinal center B cells and plasma cell precursors in the blood of children with systemic lupus erythematosus. *J. Immunol.* **167**, 2361–2369 (2001).
32. Dorner, T. & Lipsky, P. E. Correlation of circulating CD27^{high} plasma cells and disease activity in systemic lupus erythematosus. *Lupus* **13**, 283–289 (2004).
33. Rubtsov, A. V. et al. Toll-like receptor 7 (TLR7)-driven accumulation of a novel CD$11c^+$ B-cell population is important for the development of autoimmunity. *Blood* **118**, 1305–1315 (2011).
34. Wang, S. et al. IL-21 drives expansion and plasma cell differentiation of autoreactive CD$11c^{hi}$T-bet$^+$ B cells in SLE. *Nat. Commun.* **9**, 1758 (2018).
35. Blanco, P. et al. Increase in activated CD8^+ T lymphocytes expressing perforin and granzyme B correlates with disease activity in patients with systemic lupus erythematosus. *Arthritis Rheum.* **52**, 201–211 (2005).
36. Chang, A. et al. In situ B cell-mediated immune responses and tubulointerstitial inflammation in human lupus nephritis. *J. Immunol.* **186**, 1849–1860 (2011).
37. Rao, D. A. et al. Pathologically expanded peripheral T helper cell subset drives B cells in rheumatoid arthritis. *Nature* **542**, 110–114 (2017).
38. Peti-Peterdi, J. High glucose and renin release: the role of succinate and GPR91. *Kidney Int.* **78**, 1214–1217 (2010).

Acknowledgements

The authors thank C. Kusminski and R. Gordillo for helping with the metabolic Seahorse experiments. We also thank N. Baldwin, R. Marches and especially our study subjects, healthy donors and their parents. This work was supported by NIH grants P50 AR054083-01 and U19 AIO82715 (V.P.), by the Baylor Scott & White Health Care Research Foundation and by the Drukier Institute for Children's Health at Weill Cornell Medicine.

Author contributions

S.C. performed and analyzed most of the experiments, participated in their design, provided critical discussions and co-wrote the manuscript. P.B., B.D., E.M., M.C., S.A., C.H.C. and L.W. performed and analyzed several experiments. R.B., Z.X. and D.T.V perfomed gene expression and ATAC-seq analyses. J. Baisch coordinated the sample drawing and institutional review board–related issues. T.W., M.P., L.N., K.S., J.F. and J.Z. provided subject samples and data. D.U. supervised the ATAC-seq analyses. H.U. provided help designing experiments with T_{FH} cells. J. Banchereau provided critical suggestions and discussions throughout the study and contributed to writing the manuscript. V.P. conceived and supervised this study, was involved in the design and evaluation of all experiments and wrote the manuscript with comments from co-authors.

Competing interests

V.P. has received a research grant and consulting honorarium from Sanofi-Pasteur.

Additional information

Supplementary information is available for this paper at https://doi.org/10.1038/s41591-018-0254-9.

Reprints and permissions information is available at www.nature.com/reprints.

Correspondence and requests for materials should be addressed to V.P.

Publisher's note: Springer Nature remains neutral with regard to jurisdictional claims in published maps and institutional affiliations.

Methods

Subject samples. This study was approved by the institutional review boards of the University of Texas Southwestern Medical Center, Texas Scottish Rite Hospital for Children, Baylor Scott & White Health Care Systems, Pathologists Bio-Medical Laboratories and Weill Cornell Medical College. Informed consent was obtained from all subjects or their parents/guardians. Blood samples were obtained from individuals fulfilling the diagnosis of SLE according to the criteria established by the American College of Rheumatology. Healthy pediatric control samples were obtained via an institutional review board–approved protocol from children whose parents/guardians completed a questionnaire indicating that the child (i) had no chronic illness and (ii) had not been ill, received any vaccinations or suffered from seasonal allergies at the time of blood collection or during the month beforehand. Renal biopsies (formalin-fixed paraffin-embedded) from healthy controls ($n=6$) or from subects displaying class II ($n=4$), class III ($n=9$) or class IV ($n=8$) LN, as defined by the International Society of Nephrology/Renal Pathology Society revised LN classification criteria, who on review of records fulfilled the American College of Rheumatology revised criteria for the classification of SLE[39,40] were obtained from Pathologists Bio-Medical Laboratories (Lewisville, TX). All relevant ethical regulations were followed while conducting this work.

Flow cytometry and cell sorting. For CXCR3$^+$PD1^{hi}CD4$^+$ T cell quantification, cryopreserved cells were thawed into warm RPMI/10% FBS, washed once in cold PBS, and stained in PBS/1% BSA with the following antibodies for 45 min: anti-CD4 PE-Cy7 (clone SK3), anti-CXCR5 Alexa Fluor 647 (clone RF8B2), anti-CD45RA APC-H7 (clone H100), anti-PD1 Brilliant Violet 421 (clone EH12.2H7), anti-CD3 V500 (clone RPA-T4) and anti-CXCR3 Brilliant Violet 785 (clone GO25H7). Antibodies used in additional panels included anti-CD21 FITC (clone Bu32), anti-CD27 PE (clone M-T271), anti-IgD PerCP Cy5.5 (clone IA6-2), anti-CD38 PE-Cy7 (clone HB7), anti-CD19 AF700 (clone H1B19), anti-CD11c V450 (clone B-ly6) and anti-CD3 Brilliant Violet 650 (clone OKT3). Cells were washed in cold PBS and passed through a 70-µm filter, and data were acquired on a BD Fortessa, BD Canto II or Cytek Aurora flow cytometer. Data were analyzed using FlowJo 10.0.7. For pDC isolation, the total dendritic cell fraction was obtained from healthy buffy coats by magnetic cell sorting with the EasySep Human pan-DC Enrichment Kit (Stem Cell Technology) following the manufacturer's instructions. Highly pure (>99%) pDCs (Lin1$^-$HLA$^-$DR$^+$CD11c$^-$CD123$^+$ cells) were then isolated from this fraction by FACS with the following antibodies: anti-Lin1 FITC, anti-HLA-DR APC-H7 (clone G46-6), anti-CD11c APC (clone S-HCL-3) and anti-CD123 PE (clone 9F5). The 'Lin1' cocktail was composed of antibodies to CD3, CD14, CD16, CD19, CD20 and CD56 (BD Biosciences). Fresh peripheral blood naive CD4$^+$ T cells (>99% pure) were isolated using the EasySep Human Naive CD4$^+$ T Cell Enrichment Kit (Stem Cell Technology) following the manufacturer's instructions. Naive CD4$^+$ T cells where labeled with 5 µM CFSE (Thermo Fisher Scientific) following the manufacturer's instructions. Where described, primed (CFSE^{lo}) CD4$^+$ T cells were sorted from pDC and CD4$^+$ T cell cocultures at day 6. To remove dead cells and contaminating pDCs, 7ADD and anti-CD123 (clone 9F5), respectively, were used.

For B cell isolation, CD19$^+$ cells were obtained from healthy buffy coats by magnetic cell sorting with the EasySep Human B Cell Enrichment Kit (Stem Cell Technology). Enriched cells were then stained with anti-IgD APC (clone IgD26), anti-CD27 PE (clone M-T271) and anti-CD19 FITC (clone H1B19) and sorted as IgD$^+$CD27$^-$CD19$^+$ cells (naive), IgD$^-$CD27$^+$CD19$^+$ cells (memory) or IgD$^+$CD27$^+$CD19$^+$ cells (double positive). For blood CD4$^+$ T cell subset sorting, frozen peripheral blood mononuclear cells from individuals with SLE were stained with anti-CD4 PE-Cy7, anti-CXCR5 Alexa Fluor 647, anti-CD45RA APC-H7, anti-PD1 Brilliant Violet 421, anti-CD3 V500 and anti-CXCR3 Brilliant Violet 785 as described above. Then, CXCR3$^+$PD1^{lo}CD4$^+$ T cell, CXCR3$^-$PD1^{hi}CD4$^+$ T cell and CXCR3$^+$PD1^{hi}CD4$^+$ T cell populations were sorted from the CD3$^+$CD4$^+$CD45RA$^-$ CXCR5$^-$ cell fraction. Where described, CD3$^+$CD4$^+$CD45RA$^-$CXCR5$^+$CD4$^+$ T cells (T_{FH} cells) were also sorted for comparison. Cell sorting was performed on a BD FACSAria Fusion or BD FACSMelody cell sorter using a 100-µm nozzle. Sort gates were drawn as depicted in Supplementary Figs. 2a and 6a. Cell purity was routinely >98%. For functional analyses, cells were sorted into cold RPMI/10% FBS. For RNA analyses, sorted cells were lysed in RLT lysis buffer (Qiagen) with 1% β-mercaptoethanol (Sigma-Aldrich).

Oxidized mtDNA generation and pDC activation. Oxidized mtDNA was generated as previously described[3]. Briefly, healthy neutrophils were pre-incubated with IFN-α2β (2,000 U ml^{-1}; Schering) for 90 min at 37 °C and then extensively washed before incubation with anti-RNP IgG (50 µg ml^{-1}) purified from SLE subject sera. Neutrophil supernatants were then collected, centrifuged for 10 min at 1,400*g* and stored at −80 °C. pDCs (5×10^5 cells per well; 96-well U bottom plate) were cultured with 40% (vol/vol) oxidized mtDNA-containing neutrophil supernatants (referred to in the text as oxidized mtDNA) or with 5 µg ml^{-1} of either CpGA (ODN-2216; Invivogen) or CpGB (ODN-2006; Invivogen) for 24 h. The volume of oxidized mtDNA-containing neutrophil supernatants and the concentration of CpGA were selected on the basis of their capacity to trigger similar levels of IFN-α production by pDCs.

pDC analysis. pDCs were cultured as described in the previous section, and cytokine levels in the corresponding supernatants were measured with the Flex Set Kit (BD Biosciences). For flow cytometry analysis, cells were stained with anti-CD80 APC (clone L307), anti-CD86 PE (clone FUN-1), anti-CD83 FITC (clone HB15e), anti-CD40 PE (clone 5C3), anti-HLA-DR APC-H7 (clone G46-6), anti-CD123 PE (clone 9F5), anti-CXCR4 PE-Cy7 (clone 12G5), anti-CXCR3 Brilliant Violet 785 (clone GO25H7) or anti-CCR7 APC (clone 3D12). To assess the effect of IL-3 on cell viability, activated pDCs were treated with recombinant human IL-3 (50 ng ml^{-1}; BD Biosciences), cultured for an additional 24 h and then stained with the annexin V–apoptosis detection kit (BD Biosciences) following the manufacturer's instructions.

Migration assay. For Transwell-migration assays, 5×10^4 activated pDCs were applied in 100 µl cRPMI to 6.5-mm-diameter Transwell inserts that were separated from the lower chamber by polycarbonate membranes containing 5-µm pores (Costar). The lower compartments were filled with cRPMI and 1 µg ml^{-1} CCL19 or CCL21 (R&D Systems). Cells were then allowed to migrate through the bottom of the chamber for 18 h. The number of transmigrated cells relative to input was then measured.

CD4 T cell differentiation, activation and analysis. Freshly sorted allogeneic naive CD4$^+$ T cells (12×10^4) were cocultured with activated pDCs (pDC cell: T cell ratio of 1:6) in round-bottom 96-well culture plates for 6 d. Where described, MitoTempo (MT; 50 µM; Santa Cruz Biotechnology), rapamycin (100 nM; Santa Cruz Biotechnology) or anti-PD1 (10 µg ml^{-1}; clone EH12.2H7; BioLegend) was added during the coculture. As a control, 12×10^4 naive CD4$^+$ T cells were activated with 2 µl Dynabeads human T cell activator CD3/CD28 (Thermo Fisher Scientific) for 6 d (referred to in the text as T_H0). For intracellular cytokine staining, primed CD4$^+$ T cells were re-stimulated with 50 ng ml^{-1} PMA, 2 µg ml^{-1} ionomycin and 1 µl of GolgiPlug (BD Biosciences) for 5 h. Cells were then stained with a combination of anti-IL-10 APC (clone JES3-19F1) and anti-IFN-γ PE-Cy7 (clone B27) with Cytofix/Cytoperm Fixation and Permeabilization Solution (BD Biosciences) following the manufacturer's instructions. For re-stimulation experiments, 5×10^4 primed (CFSE^{lo}) CD4$^+$ T cells or sorted SLE subject CD4$^+$ T cells were re-stimulated with 10 µg ml^{-1} plate-bound anti-CD3 (clone OKT3; BioLegend) and 2 µg ml^{-1} soluble anti-CD28 (BioLegend) for 24 h. Cytokine levels in the corresponding supernatants were measured with the Flex Set Kit (BD Biosciences). For T-bet and HIF-1α intracellular staining, CD4$^+$ T cells were stained with anti-HIF-1α (clone 546-16; BioLegend) or anti-T-bet (clone 4B10; biolegend) with the Foxp3 fix/perm buffer set (BioLegend) following the manufacturer's instructions. Dead cells were excluded from the analysis by labeling with LIVE/DEAD fixable Aqua (Thermo Fisher Scientific) prior to fixation/permeabilization.

Proliferation assay. CD4 T cell proliferation was measured by resazurin reduction, as previously described[41]. Briefly, primed (CFSE^{lo}) CD4$^+$ T cells were seeded at 5×10^5 cells and re-stimulated with 10 µg ml^{-1} plate-bound anti-CD3 (clone OKT3; BioLegend) and 2 µg ml^{-1} soluble anti-CD28. After incubation for 20 h, medium supplemented with 40 µM resazurin was added for an additional 4 h. Resazurin reduction to resorufin was measured fluorometrically using a SpectraMax M5 (Molecular Devices). Results obtained were expressed in fluorescence arbitrary units (AU). Alternatively, proliferation was assessed by flow cytometry using the Click-IT EdU Flow Cytometry Proliferation Kit, according to the manufacturer's instructions (Thermo Fisher Scientific).

In vitro T_{FH} cell generation. Human T_{FH} cells were generated as previously described[42]. Briefly, after overnight stimulation of naive CD4$^+$ T cells with Dynabeads human T cell activator CD3/CD28 (Thermo Fisher Scientific) in complete RPMI medium, cells were transferred to 96-well plates coated with anti-CD3 and supplemented with 2 µg ml^{-1} soluble anti-CD28 (BioLegend), human recombinant IL-23 (25 ng ml^{-1}; BioLegend) and human recombinant TGFβ1 (5 ng ml^{-1}; BioLegend). After 4 d, cells were collected and used for analysis.

B cell cultures. For cocultures of B and T cells, naïve or memory B cells were cocultured with CD4$^+$ T cells (2×10^4 B cells and 2×10^4 CD4$^+$ T cells) in the presence of endotoxin-reduced SEB (500 ng ml^{-1}; Sigma-Aldrich) in cRPMI supplemented with 10% heat-inactivated FBS. Where described, anti-IL-10 (10 µg ml^{-1}; clone JES3-9D7; BioLegend LEAF purified antibody), anti-SUCNR1/GPR91 (20 µg ml^{-1}; Novus Biological), anti-IL-21R (10 µg ml^{-1}; clone 17A12; BioLegend LEAF purified antibody) or succinate (2 mM; Sigma-Aldrich) was added during the coculture. Sodium azide and other preservatives were removed from the antibody preparations by protein desalting with Zeba Spin Desalting Columns (7 K MWCO; Thermo Fisher Scientific). IgM and IgG concentrations were measured at day 12 in the corresponding supernatants with the Flex Set Kit (BD Biosciences). For T cell–independent B cell differentiation, naive B cells (5×10^4 cells) were cocultured with irradiated (77 Gy) human CD40L-transfected fibroblasts[43] (0.5×10^4 cells) in cRPMI supplemented with 10% heat-inactivated FBS. Recombinant human IL-10 (500 ng ml^{-1}; BioLegend) and/or succinate (2 mM; Sigma-Aldrich) was added during the cocultures IgG and IgM concentrations were

measured at day 12 in the corresponding supernatants with the Flex Set Kit (BD Biosciences).

Immunofluorescence microscopy. Cells were settled on poly-L-lysine-coated glass coverslips for 20 min at 37 °C, rinsed with PBS and then fixed with 4% paraformaldehyde for 20 min at room temperature. Cells were permeabilized with 0.05% Triton X-100 in PBS for 5 min at room temperature and then treated with blocking buffer (5% goat serum and 1% BSA in PBS) for 30 min at room temperature. Primary (anti-p65; catalog number ab16502; Abcam) and secondary antibody stainings were carried out in staining buffer (1% BSA in PBS). Isotype-specific anti-mouse or anti-rabbit Alexa Fluor 488 or Alexa Fluor 568 was used as the secondary antibody. Counterstaining of cell nuclei was performed with Hoechst stains (Molecular Probes). Samples were mounted with ProLong Gold Antifade Reagent (Molecular Probes) and examined with a Leica TCS SP5 confocal laser-scanning microscope equipped with a 63×/1.4 oil objective. ImageJ software (National Institutes of Health) was used for analysis. The percentage of co-localization was calculated from the Manders overlap coefficient using the ImageJ 'co-localization analysis' plug-in (National Institutes of Health).

Quantitative real-time PCR. $CD4^+$ T cells (5×10^4) were lysed with 50 µl of Cell-to-Ct lysis buffer (Thermo Fisher Scientific). Complementary DNA was directly synthesized from cell lysates with the Cell-to-Ct Kit (Thermo Fisher Scientific). Quantitative real-time PCR was performed with TaqMan Gene Expression Assays (Applied Biosystems) on a 7500 Real-Time PCR System (Applied Biosystems). For the housekeeping gene, β-actin was used.

SDS–PAGE and western blot. Cells were washed in PBS and then lysed in RIPA buffer in the presence of Halt Protease and Phosphate Inhibitor Cocktail (Thermo Fisher Scientific). Samples were incubated on ice for 30 min and then centrifuged (13,000*g* for 10 min at 4 °C). The supernatants containing the protein fraction were collected and stored at −80 °C until further analysis. Protein concentration was estimated using the BCA Kit (Thermo Fisher Scientific) following the manufacturer's instructions. Proteins (10–20 µg) were resuspended in 5× Lane Marker Reducing Sample Buffer (Thermo Fisher Scientific), boiled for 5 min at 100 °C and then subjected to electrophoresis with Mini-PROTEAN TGX Precast Gel (Bio-Rad). The proteins were then transferred to PVDF membranes with the TransBlot Turbo System (Bio-Rad), blocked for 1 h with 5% nonfat dry milk in Tris-buffered saline containing 0.1% Tween 20 (TBST) and incubated overnight at 4 °C with the primary antibodies. Anti-SUCNR1 (catalog number NBP1-00861; NovusBio), anti-GAPDH (2118; Cell Signaling), anti-pRb Ser807/811 (9308; Cell Signaling), anti-cyclin D1 (2989; Cell Signaling), anti-cyclin D2 (3741; Cell Signaling), anti-cyclin D3 (2936; Cell Signaling), anti-nitrotyrosine (9691; Cell Signaling), anti-NDUFA9 (ab110412; Abcam), anti-NDUFA8 (ab199681; Abcam), anti-SDHA (ab110412; Abcam), anti-UQCRC2 (ab110412; Abcam) and anti-ATP5A (ab110412; Abcam) were used as primary antibodies. After washing in TBST, the membranes were incubated for 1 h at room temperature with poly(HRP)-conjugated anti-rabbit or anti-mouse IgG (Thermo Fisher Scientific). ECL Plus reagents (Amersham) were used for detection. Digital images were acquired with the ChemiDoc MP System (Bio-Rad) and analyzed with Image Lab Software (Bio-Rad).

Short interfering RNA knockdown. Knockdown of TBX21 in primary human naive $CD4^+$ T cells was done using ACCELL short interfering RNA (siRNA) SMARTpool, designed and validated by Dharmacon. A nontargeting siRNA was used as negative control. Freshly sorted allogeneic naive $CD4^+$ T cells (12×10^4) were activated with pDCs (pDC:T cell ratio of 1:6) for 24 h before adding 1 µM of ACCELL siRNA. Cells were restimulated 96 h after transfection with 50 ng ml^{-1} PMA, 2 µg ml^{-1} Ionomycin and GolgiPlug (BD Biosciences) for 5 h and analyzed for intracellular cytokine production as described above. Protein knockdown was validated by flow cytometry.

Microarray analysis of pDCs. Total RNA was isolated using the RNeasy Kit (Qiagen), amplified and then labeled with the Illumina TotalPrep RNA Amplification Kit (Invitrogen). The Agilent 2100 Analyzer (Agilent Technologies) was used to assess RNA integrity. Biotinylated complementary RNA (cRNA) was hybridized to Illumina Human-6 Beadchip Array version 2 and scanned on the Illumina Beadstation 500. Fluorescent hybridization signals were assessed with Beadstudio software (Illumina), and statistical analysis and hierarchical clustering were performed with GeneSpring 7.3.1 software (Agilent Technologies).

RNA preparation and sequencing library preparation. Total RNA was isolated from cell lysates using a modified protocol for the RNAqueous Micro Total RNA Isolation Kit (Thermo Fisher Scientific), including on-column deoxyribonuclease digestion, and was analyzed for quality using the RNA 6000 Pico Kit (Agilent Technologies). For in vitro–generated $CD4^+$ T cells, poly(A)-enriched next-generation sequencing library construction was performed using the KAPA mRNA Hyper Prep Kit (KAPA Biosystems) with 500 ng of input total RNA and 9 amplification cycles according to the manufacturer's protocol. Individual libraries were quantitated via quantiative PCR using the KAPA Library Quantification Kit, Universal (KAPA Biosystems) and equimolar pooled. Final pooled libraries were sequenced on an Illumina NextSeq 500 with paired-end 75-base-pair (bp) read lengths. For ex vivo–isolated $CD4^+$ T cells, next-generation sequencing library construction was performed using the SMART-Seq v4 Ultra Low Input RNA Kit (Clontech) with 2 ng of input total RNA and 12 amplification cycles according to manufacturer's protocol to generate cDNA. Sequencing libraries were prepared using the Nextera XT DNA Library Prep Kit (Illumina) using 150 pg of cDNA according to the manufacturer's protocol. Individual libraries were quantitated using the Qubit dsDNA HS Assay Kit (Thermo Fisher Scientific) and equimolar pooled. Final pooled libraries were sequenced on an Illumina NextSeq 500 with paired-end 75-bp read lengths.

RNA sequencing data processing and analysis. Quality control of raw reads was performed with FASTQC. Reads were aligned to the reference human genome (GRCh38) using hisat2 after quality and adapter trimming by cutadapt. After sorting binary alignment map files by name using samtools, the HTSeq-count program was used to quantify total numbers of read counts mapped to the genome. The RNA sequencing data analysis was performed in the R programming language. The DESeq2 R package was used for size factor and dispersion estimation calculation and differential gene expression analysis.

ATAC-seq library generation and sequencing. Assay for transposase accessible chromatin sequencing (ATAC-seq) was performed as previously described[30]. Unfixed nuclei (20,000) were tagged using Tn5 transposase (Nextera DNA Sample Prep Kit; Illumina) for 30 min at 37 °C, and the resulting library fragments were purified using a MinElute Kit (Qiagen). Libraries were amplified by 10–12 PCR cycles, purified using a PCR Cleanup Kit (Qiagen) and finally sequenced on an Illumina HiSeq 2500 with 75-bp paired-end reads to a minimum depth of 30 million reads per sample. At least two technical replicates were processed per biological sample.

ATAC-seq preprocessing and bioinformatics analysis. Reads were trimmed using trimmomatic[44] and mapped to the GRCh37/hg19 assembly of the human genome using bwa-mem[45]. Duplicate reads were removed using samtools, and technical replicates were merged into a single binary alignment map file. Peak calling was performed using MACS2 with the paramters '--nomodel --shift 37 --extsize 73 --broad', and only peaks with $q < 0.05$ were selected. Peaks overlapping blacklisted regions as defined by the ENCODE project were discarded. Consensus peaks present in at least two samples were obtained using the DiffBind R package. Peaks were annotated to the closest transcription start sites in the University of California, Santa Cruz, hg19 knownGene transcriptome using the ChIPSeeker R package[46]. Peaks with differential chromatin accessiblility were found using a generalized linear model in EdgeR using the population as covariate. Genome tracks of read coverage per bp and per million mapped reads were generated using HOMER[47] makeUCSCfile with the parameters '--res 1 --norm 1e6' and were visualized with the IGV genome browser.

mtROS detection. Primed ($CFSE^{lo}$) $CD4^+$ T cells were sorted and loaded for 30 min at 37 °C with MitoSox Red (2.5 µM; Thermo Fisher Scientific) and MitoTraker Deep Red (25 nM; Thermo Fisher Scientific). Cells were then re-stimulated with 10 µg ml^{-1} plate-bound anti-CD3 (clone OKT3; BioLegend) and 2 µg ml^{-1} soluble anti-CD28 (BioLegend) for 1 h. Cells were then washed and subjected to flow cytometry analysis or immunofluorescence microscopy. Alternatively, total peripheral blood mononuclear cells from healthy donors or individuals with SLE were loaded for 30 min at 37 °C with MitoSox Red (2.5 µM; Thermo Fisher Scientific). Cells where then stained as described above and analyzed by flow cytometry.

Succinate assay. Succinate was measured with the Succinate Colorimetric Assay Kit (Abcam) following the manufacturer's instructions. Briefly, 5×10^4 $CD4^+$ T cells were homogenized with 50 µl succinate assay buffer for 5 min on ice; 10 µl of lysates was then used for the assay.

Seahorse assays. Complex I– and complex II–linked mitochondrial respiration was determined using a modified version of a previously described method[48]. Briefly, XF-24 cell culture microplates (Seahorse Bioscience) were coated with Cell-Tak (50 µL at 22.4 µg mL^{-1}; Corning), and primed ($CFSE^{lo}$) $CD4^+$ T cells (15×10^4) were plated in MAS-BSA assay solution (220 mM mannitol, 70 mM sucrose, 10 mM KH_2PO_4, 5 mM $MgCl_2$, 2 mM HEPES, 1 mM EGTA, 0.2% fatty acid–free BSA) containing XF Plasma Membrane Permeabilizer (2 nM; Seahorse Bioscience) and ADP (4 mM; Santa Cruz Biotechnology). Complex I activity was assessed by measuring the oxygen consumption rate (OCR) in response to the complex I substrate pyruvate (10 mM; Sigma-Aldrich). Malate (5 mM; Sigma-Aldrich) was added together with pyruvate to allow oxaloacetate production and condensation with acetyl coenzyme A, allowing normal pyruvate dehydrogenase flux[48]. Complex II (succinate dehydrogenase, SDH) activity was assessed by measuring the OCR in response to the complex I substrate succinate (10 mM; Sigma-Aldrich). Rotenone (2 µM; Sigma-Aldrich) was added togheter with succinate to prevent accumulation of oxaloacetate, which is a potent inhibitor of SDH[48]. For maximal respiration

rate measurement, the assay was performed in Seahorse medium (DMEM supplemented with 2 mM glutamine, 25 mM glucose and 1 mM pyruvate). Maximal respiration rate was defined as the OCR after the addition of oligomycin (2 µM; Sigma-Aldrich) and FCCP (2 µM). All extracellular flux analyses were performed using an XF-24 Extracellular Flux Analyzer (Seahorse Bioscience) as recommended by the manufacturer.

Immunofluorescence of paraffin-embedded kidney sections. Tissue sections were deparaffinized in xylene for 10 min, washed with 100% ethanol followed by 95%, 80%, 70% and 50% ethanol, and then rinsed in distilled water. For antigen retrieval, tissue sections were boiled for 10 min in 10 mM sodium citrate buffer (pH 6.0) containing 0.05% Tween 20. After two washes with distilled water and two washes with PBS, tissue sections were permeabilized for 30 min at room temperature in PBS/0.1% Triton X-100. Sections were blocked for 1 h at room temperature in blocking buffer (PBS/1% BSA/0.5% Fish Gelatin/5% goat serum) and then incubated overnight at 4 °C with the primary antibody diluted in blocking buffer. Anti-CD3 (clone OKT3; biolegend), anti-IL-10 (Clone A47-25-17; Abcam), anti-IFN-γ (catlog number ab25101; Abcam), anti-nitrotyrosine (catalog number ab42789; Abcam), anti-CD20 (clone EP459Y; Abcam), anti-CD4 (clone EPR6855; Abcam), anti-PD1 (clone EPR4877; Abcam) and anti-aquaporin1 (clone B-11; Santa Cruz Biotechnology) were used as primary antibodies. Tissue sections were then probed with Alexa Fluor–conjugated secondary antibodies, diluted in blocking buffer, at room temperature for 60 min. Counterstaining of cell nuclei in tissue sections was performed with the Hoechst stains (Thermo Fisher Scientific). Samples were then mounted with ProLong Gold Antifade Reagent (Thermo Fisher Scientific). Digital images were taken using an LSM 880 confocal microscope with an Airyscan High Resolution Detector (Carl Zeiss Microscopy). ImageJ software (National Institutes of Health) was used for data analysis.

Serum immunoglobulin levels. Serum levels of IgG and IgA were measured with total human IgG and IgA Flex Set Kits (BD Biosciences) in accordance with the manufacturer's instructions.

Statistical analysis. No specific statistical methods were used to predetermine sample size. All results are presented as the mean ± s.e.m. The significance of the difference between groups was analyzed as described in the figure legends. Pearson's correlation coefficients with two-tailed *P* values were determined in the analysis of correlations. *P* values < 0.05 were considered statistically significant. All statistical analyses were performed using GraphPad Prism Software version 7.0e.

Reporting Summary. Further information on research design is available in the Nature Research Reporting Summary linked to this article.

Data availability

Expression array data from pDCs is available at the Gene Expression Omnibus (GEO) database under accession GSE93679. Expression array data from in vitro–generated $CD4^+$ cells is available at the GEO database under accession GSE118951. Expression array data from ex vivo–isolated $CD4^+$ cells is available at the GEO database under accession GSE109843. ATAC-seq data is available at the GEO database under accession GSE110017. Uncropped data for Supplementary Fig. 2g can be accessed in Supplementary Fig. 8a. All other relevant data are available from the corresponding author directly.

References

39. Weening, J. J. et al. The classification of glomerulonephritis in systemic lupus erythematosus revisited. *Kidney Int.* **65**, 521–530 (2004).
40. Hochberg, M. C. Updating the American College of Rheumatology revised criteria for the classification of systemic lupus erythematosus. *Arthritis Rheum.* **40**, 1725 (1997).
41. Anoopkumar-Dukie, S. et al. Resazurin assay of radiation response in cultured cells. *Br. J. Radiol.* **78**, 945–947 (2005).
42. Schmitt, N. et al. The cytokine TGF-β co-opts signaling via STAT3-STAT4 to promote the differentiation of human TFH cells. *Nat. Immunol.* **15**, 856–865 (2014).
43. Garrone, P. et al. Fas ligation induces apoptosis of CD40-activated human B lymphocytes. *J. Exp. Med.* **182**, 1265–1273 (1995).
44. Bolger, A. M., Lohse, M. & Usadel, B. Trimmomatic: a flexible trimmer for Illumina sequence data. *Bioinformatics* **30**, 2114–2120 (2014).
45. Li, H. & Durbin, R. Fast and accurate short read alignment with Burrows-Wheeler transform. *Bioinformatics* **25**, 1754–1760 (2009).
46. Yu, G., Wang, L. G. & He, Q. Y. ChIPseeker: an R/Bioconductor package for ChIP peak annotation, comparison and visualization. *Bioinformatics* **31**, 2382–2383 (2015).
47. Heinz, S. et al. Simple combinations of lineage-determining transcription factors prime *cis*-regulatory elements required for macrophage and B cell identities. *Mol. Cell* **38**, 576–589 (2010).
48. Salabei, J. K., Gibb, A. A. & Hill, B. G. Comprehensive measurement of respiratory activity in permeabilized cells using extracellular flux analysis. *Nat. Protoc.* **9**, 421–438 (2014).

nature research

Corresponding author(s): Virginia Pascual

Reporting Summary

Nature Research wishes to improve the reproducibility of the work that we publish. This form provides structure for consistency and transparency in reporting. For further information on Nature Research policies, see Authors & Referees and the Editorial Policy Checklist.

Statistical parameters

When statistical analyses are reported, confirm that the following items are present in the relevant location (e.g. figure legend, table legend, main text, or Methods section).

n/a	Confirmed	
☐	☒	The exact sample size (*n*) for each experimental group/condition, given as a discrete number and unit of measurement
☐	☒	An indication of whether measurements were taken from distinct samples or whether the same sample was measured repeatedly
☐	☒	The statistical test(s) used AND whether they are one- or two-sided *Only common tests should be described solely by name; describe more complex techniques in the Methods section.*
☒	☐	A description of all covariates tested
☒	☐	A description of any assumptions or corrections, such as tests of normality and adjustment for multiple comparisons
☐	☒	A full description of the statistics including central tendency (e.g. means) or other basic estimates (e.g. regression coefficient) AND variation (e.g. standard deviation) or associated estimates of uncertainty (e.g. confidence intervals)
☒	☐	For null hypothesis testing, the test statistic (e.g. *F*, *t*, *r*) with confidence intervals, effect sizes, degrees of freedom and *P* value noted *Give P values as exact values whenever suitable.*
☒	☐	For Bayesian analysis, information on the choice of priors and Markov chain Monte Carlo settings
☒	☐	For hierarchical and complex designs, identification of the appropriate level for tests and full reporting of outcomes
☐	☒	Estimates of effect sizes (e.g. Cohen's *d*, Pearson's *r*), indicating how they were calculated
☐	☒	Clearly defined error bars *State explicitly what error bars represent (e.g. SD, SE, CI)*

Our web collection on statistics for biologists may be useful.

Software and code

Policy information about availability of computer code

Data collection	BD FACSDiva Software (v8.0.1), BD FACSChorus Software (v1.0) and Cytek SpectroFlo Software (v1.1) were used for flow data collection.
Data analysis	Statistical analysis was performed using GraphPad Prism v7.0. Flow cytometry data were analyzed with FlowJo v10.4.2. Microarray data were analyzed with GeneSpring v7.3.1. Softwares used in RNAseq and ATACseq data analysis: Trimmomatic (v0.33), Samtools (v0.1.19), bwa-mem (v0.7.12), MACS (v2.1.0), R (v3.3.1), DiffBind (v2.0.9), EdgeR (v3.14.0), HOMER (v4.6), IGV (v2.3.77) and DESeq2 (v1.16.1).

For manuscripts utilizing custom algorithms or software that are central to the research but not yet described in published literature, software must be made available to editors/reviewers upon request. We strongly encourage code deposition in a community repository (e.g. GitHub). See the Nature Research guidelines for submitting code & software for further information.

Data

Policy information about availability of data

All manuscripts must include a data availability statement. This statement should provide the following information, where applicable:

- Accession codes, unique identifiers, or web links for publicly available datasets
- A list of figures that have associated raw data
- A description of any restrictions on data availability

Gene expression (microarray data) from plasmacytoid Dendritic Cells (pDCs) is available at the Gene Expression Omnibus (GEO) GSE93679. Gene expression (RNAseq) data from in vitro generated CD4+ cells is available at the GEO database under GSE118951. Gene expression (RNAseq) data from ex vivo isolated CD4+ cells is available at the GEO database under accession GSE109843. ATAC-sequencing data is available at the GEO database under accession GSE110017. Uncropped data for Supplementary Fig. 2g can be accessed in Supplementary Fig. 8a. All other relevant data are available from the corresponding author directly.

Field-specific reporting

Please select the best fit for your research. If you are not sure, read the appropriate sections before making your selection.

☒ Life sciences ☐ Behavioural & social sciences ☐ Ecological, evolutionary & environmental sciences

For a reference copy of the document with all sections, see nature.com/authors/policies/ReportingSummary-flat.pdf

Life sciences study design

All studies must disclose on these points even when the disclosure is negative.

Sample size	Samples were chosen based on availability of patient material. No sample size calculation was performed a priori. Up to eighty percent of pediatric SLE patients develop nephritis (LN). Thus, a sample size of 30 should include enough patients with and without this complication. We did enroll 27 pediatric SLE patients in our study. Twenty of them were diagnosed with LN and 7 did not. This number of patients enabled us to find statistically significant correlations with the cell populations of interest and the parameters that we analyzed.
Data exclusions	No data were excluded from the analyses.
Replication	All in vitro assays were performed at least three times with different donors. The data presented is representative of one assay. All attempts at replication were successful.
Randomization	SLE patients were allocated into different experimental groups according to the presence or absence of nephritis and the nephritis class defined by the International Society of Nephrology/Renal Pathology Society revised LN classification criteria.
Blinding	Kidney imaging acquisition and analyses were performed blinded in terms of Lupus nephritis class.

Reporting for specific materials, systems and methods

Materials & experimental systems

n/a	Involved in the study
☒	☐ Unique biological materials
☐	☒ Antibodies
☐	☒ Eukaryotic cell lines
☒	☐ Palaeontology
☒	☐ Animals and other organisms
☐	☒ Human research participants

Methods

n/a	Involved in the study
☒	☐ ChIP-seq
☐	☒ Flow cytometry
☒	☐ MRI-based neuroimaging

Antibodies

Antibodies used	anti-CD4 PE-Cy7 (Clone SK3) - BD Biosciences – cat#557852 anti-CXCR5 AlexaFluor 647 (Clone RF8B2) - BD Biosciences – cat#558113 anti-CD45RA APC-H7 (Clone H100) - BD Biosciences – cat#560674 anti-PD1 Brilliant Violet 421 (Clone EH12.2H7) – Biolegend – cat#329919 anti-CD3 V500 (Clone RPA-T4) - BD Biosciences – cat#560770

anti-CXCR3 Brilliant Violet 785 (Clone GO25H7) – Biolegend – cat#353737
anti-CD21 FITC (Clone Bu32) – Biolegend – cat#354909
anti-CD27 PE (Clone M-T271) – Biolegend – cat#356405
anti-IgD PerCP Cy5.5 (Clone IA6-2) – Biolegend – cat#348207
anti-CD38 PE-Cy7 (Clone HB7) - BD Biosciences – cat#335790
anti-CD19 AF700 (Clone H1B19) – Biolegend – cat#302225
anti-CD11c V450 (Clone B-ly6) - BD Biosciences – cat#560369
anti-CD3 Brilliant Violet 650 (Clone OKT3) – Biolegend – cat#317323
anti-Lin1 FITC - BD Biosciences - cat #340546
anti-HLADR APC-H7 (Clone G46-6) - BD Biosciences – cat#561358
anti-CD11c APC (Clone S-HCL-3) - BD Biosciences – cat#340544
anti-CD123 PE (Clone 9F5) - BD Biosciences – cat#340545
anti-IgD APC (Clone IgD26) – Miltenyi – cat#130-099-221
anti-CD27 PE (Clone MT271) – Biolegend – cat#356405
anti-CD19 FITC (Clone H1B19) - BD Biosciences – cat#560994
anti-CD80 APC (Clone L307) - BD Biosciences – cat#561134
anti-CD86 PE (Clone FUN-1) - BD Biosciences – cat#555658
anti-CD83 FITC (Clone HB15e) – Biolegend – cat#305305
anti-CD40 PE (Clone 5C3) – Biolegend – cat#334307
anti-HLADR APC-H7 (Clone G46-6) - BD Biosciences – cat#561358
anti-CXCR4 PECy7 (Clone 12G5) – Biolegend – cat#306513
anti-CXCR3 Brilliant Violet 785 (Clone GO25H7) – Biolegend – cat#353737
anti-CCR7 APC (Clone 3D12) – Thermofisher – cat#17-1979-41
anti-IL10 APC (Clone JES3-19F1) – Biolegend – cat#506806
anti-IFNg PE-Cy7 (Clone B27) - BD Biosciences – cat#557643
anti-HIF1a antibody (Clone 546-16) – Biolegend– cat#359703
anti-Tbet antibody (Clone 4B10) – Biolegend – cat#644803

anti-PD1 antibody (clone EH12.2H7) – Biolegend – cat#329925
anti-CD3 (clone OKT3) – Biolegend – cat#317325
anti-CD28 mAb – Biolegend – cat#302933
anti-IL10 (clone JES3-9D7) – Biolegend – cat#501406
anti-SUCNR1/GPR91 - Novus Biological – cat#NBP1-00861SS
anti- IL21R (clone 17A12) – Biolegend – cat#359503

anti-p65 antibody – Abcam – cat#ab16502

anti-GAPDH (Cat # 2118; Cell Signaling)
anti-pRb Ser807/811 (Cat # 9308; Cell Signaling)
anti-Cyclin D1 (Cat # 2989; Cell Signaling)
anti-Cyclin D2 (Cat # 3741; Cell Signaling)
anti-Cyclin D3 (Cat # 2936; Cell Signaling)
anti-Nitrotyrosine (Cat # 9691; Cell Signaling)
anti-NDUFA9 (Cat # ab110412; Abcam)
anti-NDUFA8 (Cat # ab199681; Abcam)
anti-SDHA (Cat # ab110412; Abcam)
anti-UQCRC2 (Cat # ab110412; Abcam)
anti-ATP5A (Cat # ab110412; Abcam)

anti-CD3 (Clone OKT3; Biolegend) cat#317325
anti-IL10 (Clone A47-25-17; Abcam) cat#ab134742
anti-IFNg (Cat #ab25101; Abcam)
anti-Nitrotyrosine (Cat #ab42789; Abcam)
anti-CD20 (Clone EP459Y; Abcam) cat#ab78237
anti-CD4 (Clone EPR6855; Abcam) cat#ab133616
anti-PD1 (Clone EPR4877; Abcam) cat#ab137132
anti-Aquaporin1 (Clone B-11; SantaCruz) cat#sc-25287

Validation

Each antibody was validated accordingly to the manufacturer instructions. Were not stated differently, 1:1000 dilution for the antibodies was used.

Eukaryotic cell lines

Policy information about cell lines

Cell line source(s)

Human CD40L-transfected murine fibroblasts were obtained from the the laboratory of Dr. Jacques Banchereau. See Methods section for details.

Authentication

Cell lines were authenticated by assessing their ability to induce B cell proliferation and activation.

Mycoplasma contamination

All cell lines tested negative for mycoplasma contamination.

Commonly misidentified lines (See ICLAC register)	No commonly misidentified cell lines were used.

Human research participants

Policy information about studies involving human research participants

Population characteristics	On average, our SLE patient population is 86% female and 14% male (female patients: age range: 8-17 y/o, with an average age of 14; 58% Hispanic/White, 35% non-Hispanic/African American, 5% non-Hispanic/White, 2% other; male patients: age range 9-17 y/o, with an average age of 12 years; 57% Hispanic/White, 14% non-Hispanic/African American, 2% other).
Recruitment	The SLE patient population was recruited from pediatric rheumatology clinics at Texas Scottish Rite Hospital for Children and Children's Medical Center, both in Dallas, Texas; and as such is representative of the lupus patients in that geographic region of the country.

Flow Cytometry

Plots

Confirm that:

☒ The axis labels state the marker and fluorochrome used (e.g. CD4-FITC).

☒ The axis scales are clearly visible. Include numbers along axes only for bottom left plot of group (a 'group' is an analysis of identical markers).

☒ All plots are contour plots with outliers or pseudocolor plots.

☒ A numerical value for number of cells or percentage (with statistics) is provided.

Methodology

Sample preparation	See Methods section for details.
Instrument	BD FascAria II, BD Fortessa, BD FacsCanto II and BD FacsMelody (BD Biosciences). Cytek Aurora (Cytek).
Software	BD FACSDiva Software (v8.0.1), BD FACSChorus Software (v1.0) and Cytek SpectroFlo Software (v1.1) were used for flow data collection. Flow cytometry data were analyzed with FlowJo v. 10.4.2.
Cell population abundance	See Main text and Methods sections for details.
Gating strategy	See Main text and Methods sections for details.

☒ Tick this box to confirm that a figure exemplifying the gating strategy is provided in the Supplementary Information.